Earth and Planetary Science Letters 363 (2013) 168–180

Contents lists available at SciVerse ScienceDirect

Earth and Planetary Science Letters

journal homepage: www.elsevier.com/locate/epsl

First archeointensity determinations on Maya incense burners from Palenque temples, Mexico: New data to constrain the Mesoamerica secular variation curve

G. Fanjat [a], P. Camps [a,*], L.M. Alva Valdivia [b], M.T. Sougrati [d], M. Cuevas-Garcia [c], M. Perrin [e]

[a] Géosciences Montpellier, CNRS and Université de Montpellier 2, Montpellier, France
[b] Laboratorio de Paleomagnetismo, Instituto de Geofísica, Universidad Nacional Autonoma de Mexico, México D.F., Mexico
[c] Instituto Nacional de Antropologia e Historia, México D.F., Mexico
[d] Institut Charles Gerhardt, Laboratoire des Agrégats, Interfaces et Matériaux pour l'Energie, 34095 Montpellier, France
[e] AIx-Marseille Université, CNRS, IRD, CEREGE UM34, 13545 Aix en Provence, France

ARTICLE INFO

Article history:
Received 15 May 2012
Received in revised form
16 November 2012
Accepted 27 December 2012
Editor: Y. Ricard

Keywords:
archeointensity
secular variation
Palenque
incense burner

ABSTRACT

We present archeointensity data carried out on pieces of incense burners from the ancient Maya city of Palenque, Chiapas, Mexico, covering much of the Mesoamerican Classic period, from A.D. 400 to A.D. 850. We worked on pieces from 24 incense burners encompassing the five Classic ceramic phases of Palenque: Motiepa (A.D. 400–500), Cascadas (A.D. 500–600), Otulum (A.D. 600–700), Murcielagos (A.D. 700–770), and Balunté (A.D. 770–850). All the samples come from highly elaborate, flanged pedestal of incense burners that are undoubtedly assigned to a ceramic phase by means of their iconographic, morphological and stylistic analyses. Archeointensity measurements were performed with the Thellier–Thellier's method on pre-selected samples by means of their magnetic properties. We obtained archeointensities of very good technical quality from 19 of 24 pieces, allowing the determination of a precise mean value for each ceramic phase, between 29.1 ± 0.9 μT and 32.5 ± 1.2 μT. The firing temperatures of ceramics were estimated with Mössbauer spectroscopy between 700 °C and 1000 °C. These values ensure that a full thermo-remanent magnetization was acquired during the original heating. Our results suggest a relative stability of the field intensity during more than 400 years in this area. The abundance of archeological material in Mesoamerica contrasts with the small amount of archeomagnetic data available that are, in addition, of uneven quality. Thus, it is not possible to establish a trend of intensity variations in Mesoamerica, even using the global databases and secular variation predictions from global models. In this context, our high technical quality data represent a strong constraint for the Mesoamerican secular variation curve during the first millennium AD. The corresponding Virtual Axial Dipole Moments (VADM) are substantially smaller than the ones predicted by the last global geomagnetic models CALS3k.4, suggesting the need for additional data to develop a regional model and a reference curve for Mesoamerica.

1. Introduction

Records in volcanic rocks and baked clays of the ancient geomagnetic field intensity over geological time (paleointensity) and over pre-historical and historical time (archeointensity) are unique observations of the temporal evolution of the energy involved in dynamo processes occurring in the Earth's liquid outer core. Archeomagnetic measurements represent a significant part of data over the last 10 millennia, extending in the past the historical records from sailors and the continuous direct data acquisition in magnetic observatories and from satellites. Indeed, archeological artifacts made from baked clays such as pottery, kilns, bricks or any other burnt clay structures offer an opportunity to recover the direction and/or the intensity of the ancient field as they usually carry a strong and stable thermo-remanent magnetization (TRM) acquired during their last firing. Hence, they could provide a long and accurate record over the last millennia of the geomagnetic field and its secular variation (e.g. compilations of Genevey et al., 2008; Donadini et al., 2009). Global inverse models, in which the Gauss coefficients up to degree 10 are recovered from the experimental data, have been built to millennial time scales. The latest ones CALSxk (Continuous model of Archeomagnetic and Lake Sediment data over the x last millennia)

* Corresponding author. Tel.: +33 467 14 39 38.
E-mail addresses: camps@gm.univ-montp2.fr, pcamps@univ-montp2.fr (P. Camps).

0012-821X/$ - see front matter © 2013 Elsevier B.V. All rights reserved.
http://dx.doi.org/10.1016/j.epsl.2012.12.035

and ARCH3k (relying on a selective compilation of only archeomagnetic data) are defined for the time intervals of 3 and 10 kyrs (Donadini et al., 2010; Korte and Constable, 2011; Korte et al., 2011). These mathematical models are purely descriptive. Yet, they represent a double interest (Gallet et al., 2009). The first concerns the geophysical research. They allow one to challenge the robustness of our prevailing knowledge on the geomagnetic field fluctuations. Furthermore, they permit an examination of several questions as varied as the role of the geomagnetic field on the cosmogenic isotopes production rate (Lifton et al., 2008) or the possible transfer of energy from the geomagnetic dipole to the non-dipole terms when the field fluctuates (Camps and Prévot, 1996). The second concerns the archeometry. Well-established data sets from different regions of the world are necessary to develop dating methods by comparing the geomagnetic field elements (intensity and/or direction) as recorded by an archeological artifact against a master curve of the secular variation of the geomagnetic field (e.g. Lanos et al., 2005; Pavón-Carrasco et al., 2011). The precision of archeomagnetic dating depends directly on the accuracy of the calibration curves. However, a common deficiency in all of these models is a large spatial bias arising from the fact that most of data comes from the northern hemisphere, essentially from Europe, linked to a lack of reliable intensity and directional data from the southern hemisphere (Hongre et al., 1998; Valet et al., 2008; Nilsson et al., 2010). Indeed, numerous regional studies have provided high quality archeomagnetic data in several parts of Europe (e.g. compilations of Gallet et al., 2002; Kovacheva et al., 2009; Tema et al., 2010; Tema and Kondopoulou, 2011), because the cultural heritage is very important and numerous investigations have been carried out. These compilations have been used to build regional master curves that allow a precise dating of archeological artifacts (Kovacheva et al., 2004; Gallet et al., 2009; Aidona and Kondopoulou, 2012).

Surprisingly enough, the secular variation curve of the geomagnetic field in Mesoamerica is rather poorly defined despite the important amount of archeological sites and the impressive cultural heritage. Data are sparse and are of uneven quality. As a consequence, archeomagnetic dating in Mesoamerica is still a hard task to manage (López-Téllez et al., 2008). Indeed, after the pioneering studies of Nagata et al. (1965) and Bucha et al. (1970), very few studies were performed on archeological artifacts until recently (Ceja et al., 2009; Morales et al., 2009; Alva-Valdivia et al., 2010; Pineda-Durán et al., 2010, 2011) and on historical lava flows (Gonzalez et al., 1997; Morales et al., 2001; Alva-Valdivia, 2005; Conte-Fasano et al., 2006). The present study is part of this recent effort. We carried out an archeointensity study of 24 incense burners excavated in the Maya city of Palenque (Mexico). Our sampling covers a large part of the Classic period, from 400 A.D. to 850 A.D.

In the first part of this paper, we will describe the samples in their archeological context. Then, following the analysis of the magnetic mineralogy we will present the archeointensity experiments and results. Next, in order to strengthen the archeointensity determinations, we will try to estimate the firing conditions of the incense burners during their manufacture. Finally, we will discuss the reliability of these results, and a comparison with an appropriate data selection from the Mesoamerican region, and with global models will be attempted.

2. Archeological context and description of the samples

The ceramics being considered in this study are pieces of incense burners excavated at the archeological site of Palenque, Mexico. This ancient Maya city, located in the central lowland of the Maya territory (Fig. 1), was one of the most important cities

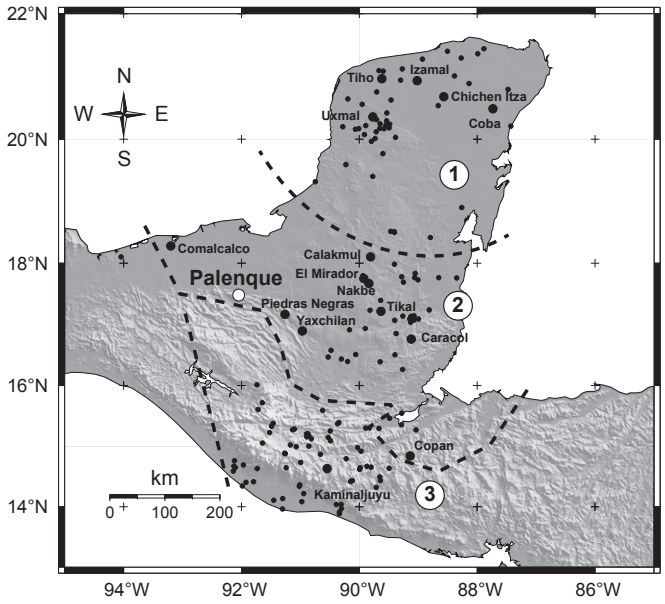

Fig. 1. Map of the Maya region showing locations of some of the principal cities (filled circles). Bigger symbols and labels are plotted for the most important cities. The thick dashed lines delimit the northern lowlands (1), the central lowlands (2), and the highlands and Pacific coast (3) cities.

during the Classic period of Maya civilization (250 A.D.–900 A.D.). Incense burners were one of the main components of the religious paraphernalia in the Palenque region and were composed of two parts: a hollow cylindrical pedestal (Fig. 2) surmounted by a conical receptacle for burning incense. Rice (1999) distinguished two groups of incense burners, with effigy and without effigy. The effigy incense burners are highly embellished with the representation of divinities on the pedestal (Fig. 2). The discovery of about 100 effigy incense burners in the group of Temples of the Cross in Palenque is an unprecedented event in the Mayan area.

These iconographically rich objects appear to be a potentially good material for archeointensity determinations for two main reasons. First, they are undoubtedly locally made, at Palenque or in its immediate vicinity (Rands et al., 1979). Palenque was a peripheral Classic Maya site (Fig. 1) exhibiting local particularities in art and ceramic traditions. Rands et al. (1979) noted that the incense burners excavated at Palenque are quite distinctive in both shape and decoration from those found in other parts of Mesoamerica. A further evidence is given by their compositional analysis (Bishop et al., 1982) in regard to the geological environment of the ancient city, which is located in the first limestone foothills that rise steeply from the alluvial Tabasco–Chiapas plain. Crushed limestone and quartz sand usually added as tempering materials in clay paste are present around Palenque city, and both were utilized in the ceramic manufacture. Second, and perhaps the main reason is that Palenque incense burners are perfectly well dated within reasonably short time intervals by means of iconographic, morphological, stylistic analyses and manufacturing technology, in conjunction with architectural stratigraphy and epigraphy.

2.1. Stratigraphic information

Most of the elaborately decorated flanged cylindrical pedestals were found buried under clay and stones in the basement of the main temples. Almost all of them have been unearthed broken and partly altered because of the absence of container. The ritual practice of burying is now well understood (Cuevas-García, 2007). Then, by means of the analysis of the archeological context, the

Fig. 2. Two incense burner pedestals from (a) Temple of the Foliated Cross (TCF-13/93, Balunté ceramic phase) and (b) Temple of the Cross (TC-5/93, Otulum ceramic phase), from Cuevas-García (2007).

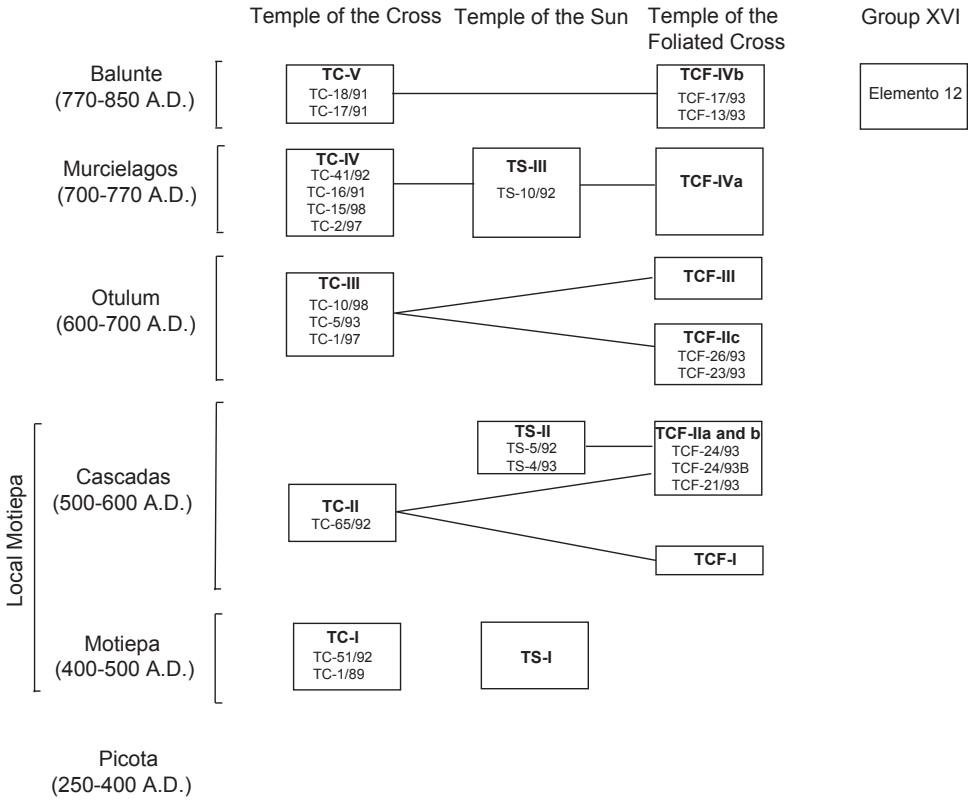

Fig. 3. Schematic classification of the incense burners of the group of temples of the cross (redrawn from Cuevas-García, 2007; Rands, 2007).

specific places in the building where the incense burners were excavated yield stratigraphic information of first importance for dating. Incense burners were used to worship the gods who were represented on pedestals by burning vegetable resins and probably human blood deposited in braziers placed above. One could understand that burying in temples the incense burners representing the gods was a ritual practice of periodic renovation. This interpretation results from an ethnographic analogy relying on a study of ritual systems in Palenque and new sight-reading inscriptions (Cuevas-García, 2007). Incense burners show important symbolic properties as the fact of considering the "incense-gods" as living beings having a life cycle. Through their death and resurrection, the regeneration of the world became favorable.

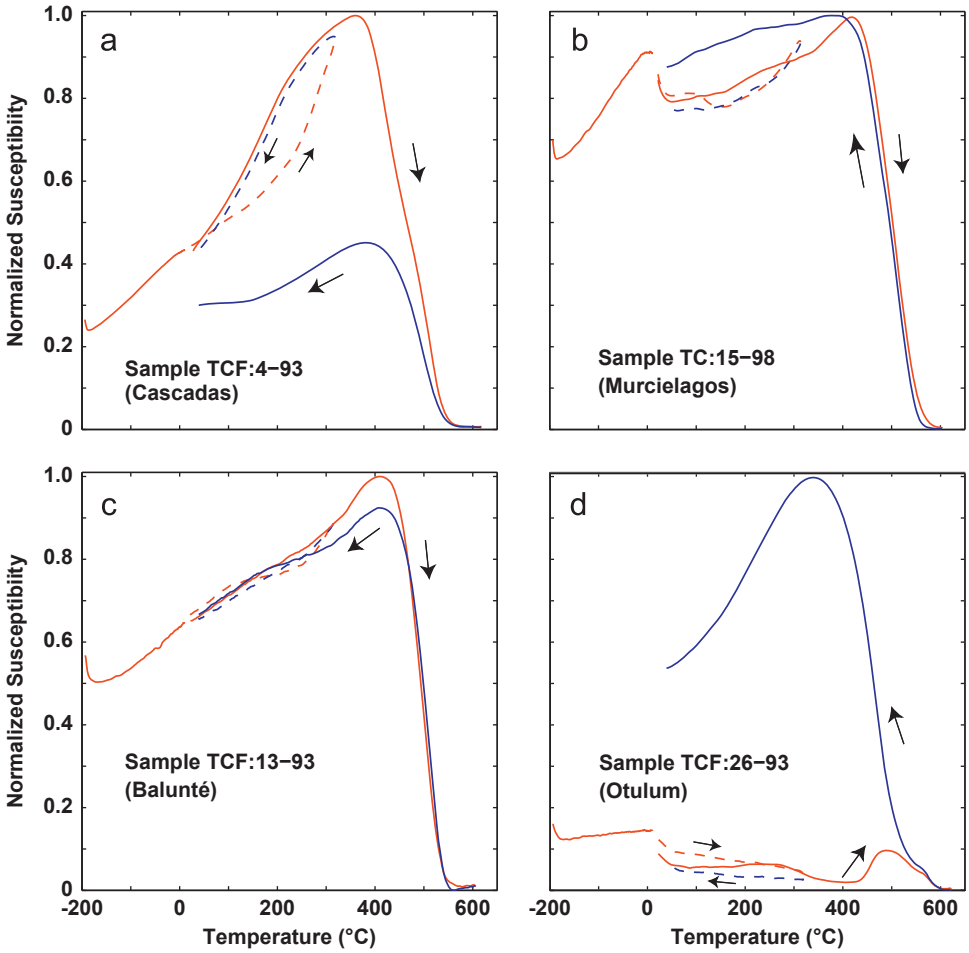

Fig. 4. Representative examples of low-field susceptibility versus temperature curves measured under air atmosphere (*K–T* curves). Susceptibility values are normalized to the maximum susceptibility. The heating curves are in red, the cooling curves are in blue. The dashed lines correspond to partial heating–cooling cycles. (For interpretation of the references to color in this figure legend, the reader is referred to the web version of this article.)

2.2. Iconographic information

During the Classic period, incense burners were produced continuously and changes in style can be established by means of criteria of evolution, the simplest artifacts attached to the earlier period and the more evolved attached to the most recent period (Cuevas-García, 2007). The most obvious principle is the height of pedestals and as a consequence, the increase in the number of iconographic patterns (Fig. 2). Applying such criteria, Cuevas-García (2007) has first established a seriation of the pedestals and then assigned for each of them, by means of a crosschecking with alternative sources of archeological information, a ceramic phase within the chronological framework for Palenque. We followed the correlation between the ceramic phases and the christian calendar as proposed by Rands (1974) and Cuevas-García (2007) (Fig. 3).

2.3. The ceramic phases of Palenque

The chronology of the history of Palenque is based on its ceramic assemblage. The Classic period in Palenque is usually divided in 5 or 6 ceramic phases. The early Classic is divided into two phases, Picota (250–400 A.D.) and Motiepa (400–500 A.D). A Middle Classic Cascadas (500-600 A.D.) phase was later added as a subdivision, but is still debated (Rands, 2007). The Late Classic is composed of three phases: Otulum (600–700 A.D.), Murcielagos (700–770 A.D.) and Balunté (770–850 A.D.). Distinct characteristics of the hollow flanged pedestals within each ceramic phases are the following:

1. Motiepa (400–500 A.D.): The incense burners share an identical manufacturing technique on the basis of a paste of calcite temper and dark color inside and brown outside. The size of pedestals is about 51 cm. In the iconographic motifs the deity known as GI is always represented, accompanied at the top with a head of a lizard.
2. Cascadas (500–600 A.D.): The incense burners from this phase are more numerous and are more heterogeneous than those of the previous group, especially with the use of different kinds of pastes. They present a greater height, between 61 cm and 78 cm. Some modifications in the manufacturing technique are noticed, as the use of different pastes than that used during the Motiepa phase. The god GI is still represented on the pedestals and the GIII deity is introduced. Another distinctive feature arises from the representation of the cheekbones highlighted in the faces of the deities.
3. Otulum (600–700 A.D.): This set of incense burners is quite homogeneous and show little variability. It appears that there was a hiatus in manufacturing techniques between Cascadas and Otulum ceramics. The same manufacturing technique was used, but an important increase in the height of the pieces to an average of 81 cm is observed. The GI and GIII are still represented but two variants are introduced, localized only in the Temple of the Cross, while in the Foliated Cross temple the same variant of the GIII initiated in Cascadas was kept.

4. Murcielagos (700–770 A.D.): It is a heterogeneous group of incense burners. The manufacturing technique is different from the one used in the previous phases and allows a greater volume of the masks and an higher shape, up to more than 94 cm high. Moreover, different kinds of pastes were used and one of them is very crumbly.
5. Balunté (770–850 A.D.): All hollow flanged cylinders from this phase share the same manufacturing technique and stylistic similarities, with the representation of the same deities, including variations relative to each temple. These incense burners are the largest pieces and reach 1.14 m in height.

2.4. The samples

The samples used for the archeointensity determinations are small pieces that have been preserved when the hollow flanged cylinders were restored in order to allow possible analyses. All pieces belong to pedestals for which a ceramic phase is undoubtedly identified (Cuevas-García, 2007). They usually come from the non-decorated rear part. We selected only pieces that showed a homogeneous color body (brown to brownish gray) and rejected those with a dark core. A piece was selected for 24 different hollow flanged cylinders excavated in the Temple of the Cross (13 pieces), Temple of the Cross Foliated (7 pieces), Temple of the Sun (3 pieces) and Group XVI (1 piece). For each of them, six small samples (about $5 \times 5 \times 5$ mm) were cut and packed in salt pellets in order to treat them as standard paleomagnetic samples and to proceed to archeointensity experiments.

3. Magnetic properties of samples

A good knowledge of the nature, the size and the thermal stability of the thermoremanence carriers present in the samples is essential prior to any attempt to estimate the archeointensity.

3.1. Thermomagnetic curves

Low-field susceptibility versus temperature experiments (K–T curves) allow one to determine the Curie temperature and the stability of the magnetic carriers upon heatings. Thermomagnetic curves have been performed for at least one piece from each hollow flanged pedestals at the University of Montpellier. First, a piece of archeological material was crushed in an agate mortar and sieved to collect the 0.4–0.8 mm size fraction. Then, K–T curves were acquired at low-temperature by means of a cryostat apparatus (CS-L) and at high-temperature under Argon using a furnace (CS-3) coupled to the KLY-3 Kappabridge instrument (Agico, Czech Republic). The studied material was first heated from liquid nitrogen temperature (-195 °C) to about 650 °C and cooled down to room temperature. For some samples, the low temperature measurements were repeated from liquid nitrogen temperature up to room temperature in order to see if any changes occurred. The data were corrected for the empty holder and normalized to the maximum susceptibility. Some samples were treated with several heating–cooling cycles in which the maximum temperature is progressively increased. This procedure allows one to estimate the maximum temperature at which the samples can be heated without changing their magnetic properties.

Distinct behaviors were identified (Fig. 4). In spite of different shapes, most of the curves are nearly reversible suggesting few mineralogical changes during heating at least up to 400 °C (Fig. 4). Curie temperatures were calculated using the method of the second derivative of the heating curves and vary between 500 and 580 °C. This indicates that magnetite or Ti-poor titanomagnetite is the main magnetic carriers. Hopkinson's effect, increase in susceptibility at temperatures just below the Curie temperature, is often observed (Fig. 4b and c). This behavior reflects that the Ti-poor titanomagnetites are small grains behaving as single domain or small pseudo-single domains grains, and thus, that the samples are rather well-suited for archeointensity determinations. Finally, we note that about 3% of measured samples contain a titanohematite phase (Fig. 4d), as attested by the very low initial susceptibility, which disassociates above 500 °C producing an almost pure fine-grained magnetite as is sometimes observed in volcanic rocks (e.g Hoffman et al., 2008).

3.2. Hysteresis loops

Hysteresis measurements were performed at room temperature and in fields up to 1.2 T on all studied archeological pieces by means of the AGFM Micromag apparatus of the paleomagnetic laboratory at Mexico City. The curves are symmetrical in all cases and were corrected from the paramagnetic fraction, assuming the absence of magnetic mineral of high coercivity (hematite for example). The hysteresis parameter ratios are plotted in Day's diagram (Day et al., 1977, Supplementary Fig. S1). All samples present pseudo-single domain characteristics. This observation is in close agreement with most of the K–T results.

4. Archeointensity determinations

Archeointensity measurements were carried out in the laboratory of Geosciences Montpellier, using the Thellier and Thellier (1959) procedure in its original form, with regular partial thermoremanent magnetization (pTRM) checks.

4.1. Sample selection

Samples used for absolute archeointensity determinations must satisfy the following criteria:

1. The characteristic remanent magnetization (ChRM) must be a thermoremanent magnetization not overprinted by a significant secondary component.
2. The magnetic properties of the samples must be stable during experimental heatings in the laboratory.
3. The magnetic carriers must be single-domain or pseudo-single-domain grains in order to fulfill the independence and additivity laws of partial thermoremanent magnetization (Thellier and Thellier, 1959).

According to the hysteresis parameters, magnetic carriers of most of samples present a pseudo-single-domain behavior. Then, according to K–T curves, we selected samples presenting, within a reasonable range of temperature, a stable behavior during heating to minimize thermal alteration occurring during the laboratory experiments.

4.2. Experimental procedure

Samples were heated and cooled twice for each temperature step T_i. At each temperature level T_i, the samples were cooled in the presence of a 40-μT induction field oriented along the cylinder axis of the core (z-axis) during the first cooling and in the opposite direction during the second one. Temperature steps were performed from room temperature to a maximum temperature of 500 °C. For every two temperature increments, a pTRM check was performed to detect any alteration in the

Table 1
Archeointensity results.

Sample	n	T °C (min–max)	f	g	q	DRAT (%)	H (μT)	$\mathcal{F}_{aTRM}$	H_{aTRM} (μT)	$\mathcal{F}_{CR}$	$H_{aTRM,CR}$ (μT)
Balunte A.D. 770–850											
TC:18/91-2	14	20–400	0.65	0.90	10.6	3.9	35.5 ± 1.9	n.d.	n.d.	(0.965)	n.d.
TC:18/91-3	10	100–330	0.68	0.86	14.6	3.0	38.8 ± 1.6	0.743	28.8 ± 1.2	1.007	28.6 ± 1.2
TC:18/91-4	9	130–330	0.66	0.83	80.8	2.0	29.2 ± 0.2	1.074	31.4 ± 0.2	1.007	31.1 ± 0.2
TC:17/91-3	8	140–380	0.72	0.81	18.7	7.8	46.3 ± 1.4	0.807	37.3 ± 1.1	1.042	35.9 ± 1.1
TC:17/91-4	10	100–440	0.77	0.87	13.6	8.7	37.0 ± 1.8	0.969	35.9 ± 1.7	1.012	35.4 ± 1.7
TC:17/91-5	12	100–500	0.95	0.89	8.9	5.9	41.4 ± 3.9	0.814	33.7 ± 3.2	(0.990)	33.7 ± 3.2
TC:17/91-6	8	100–355	0.65	0.81	9.1	8.9	38.3 ± 2.2	0.989	37.9 ± 2.2	1.033	36.7 ± 2.1
El 12 Gpo XVI-1	7	20–400	0.82	0.76	12.9	5.2	31.9 ± 1.6	0.980	31.3 ± 1.6	n.d.	n.d.
El 12 Gpo XVI-2	10	130–350	0.69	0.87	35.1	1.8	30.1 ± 0.5	1.050	31.6 ± 0.5	1.003	31.5 ± 0.5
El 12 Gpo XVI-3	10	100–330	0.73	0.87	48.9	0.9	28.9 ± 0.5	1.093	31.6 ± 0.5	1.013	31.2 ± 0.5
El 12 Gpo XVI-4	11	100–350	0.78	0.87	46.6	1.1	37.1 ± 0.5	0.943	35.0 ± 0.5	(0.998)	35.0 ± 0.5
El 12 Gpo XVI-5	8	100–355	0.78	0.82	45.1	1.6	29.4 ± 0.4	1.045	30.7 ± 0.4	1.042	29.5 ± 0.4
El 12 Gpo XVI-6	9	100–380	0.82	0.81	30.1	4.8	32.3 ± 0.7	n.d.	n.d.	1.029	n.d.
TCF:17/93-2	12	130–400	0.68	0.90	17.6	4.2	37.4 ± 1.3	0.827	30.9 ± 1.1	1.007	30.7 ± 1.1
TCF:17/93-3	13	130–440	0.72	0.90	34.7	8.0	40.2 ± 0.8	0.921	37.0 ± 0.7	1.009	36.7 ± 0.7
TCF:17/93-4	13	100–400	0.62	0.90	22.0	2.2	39.8 ± 1.0	0.816	32.5 ± 0.8	(0.980)	32.5 ± 0.8
TCF:13/93-2	13	100–400	0.80	0.90	21.8	4.9	35.5 ± 1.2	0.894	31.7 ± 1.1	(0.997)	31.7 ± 1.1
TCF:13/93-3	16	100–500	0.88	0.92	69.4	4.0	38.7 ± 0.4	0.822	31.8 ± 0.3	(0.962)	31.8 ± 0.3
TCF:13/93-4	10	100–330	0.75	0.87	22.6	5.4	38.0 ± 1.1	n.d.	n.d.	1.004	n.d.
Unweighted average:							36.1 ± 1.1		33.1 ± 0.7		32.8 ± 0.7
Weighted average:							32.0 ± 1.4		32.0 ± 0.7		**31.7 ± 0.7**
Murcielagos A.D. 700–770											
TC:41/92-1	6	120–400	0.68	0.74	6.9	4.9	38.6 ± 2.9	0.838	32.3 ± 2.4	n.d.	n.d.
TC:41/92-2	12	130–400	0.52	0.88	14.9	7.5	34.0 ± 1.0	0.911	31.0 ± 0.9	(0.991)	31.0 ± 0.9
TC:41/92-3	9	160–350	0.56	0.85	20.1	1.5	39.0 ± 0.9	0.824	32.1 ± 0.7	1.007	31.9 ± 0.7
TC:41/92-4	13	100–400	0.79	0.89	20.4	5.7	36.3 ± 1.3	0.848	30.8 ± 1.1	(0.985)	30.8 ± 1.1
TC:16/91-4	11	180–500	0.76	0.87	12.0	9.9	39.8 ± 2.2	0.766	30.5 ± 1.7	1.000	30.5 ± 1.7
TC:15/98-3	11	180–500	0.69	0.89	31.0	2.2	43.8 ± 0.9	0.777	34.0 ± 0.7	1.009	33.7 ± 0.7
TS:10/92-2	15	130–500	0.86	0.92	44.7	5.0	35.2 ± 0.6	0.910	32.0 ± 0.5	1.012	31.7 ± 0.5
TS:10/92-3	16	100–500	0.87	0.92	50.1	4.8	32.6 ± 0.5	0.898	29.3 ± 0.4	1.019	28.7 ± 0.4
TS:10/92-4	16	100–500	0.85	0.92	71.6	5.2	36.6 ± 0.4	0.834	30.5 ± 0.3	1.013	30.1 ± 0.3
Unweighted average:							37.3 ± 1.1		31.4 ± 0.5		31.0 ± 0.5
Weighted average:							36.0 ± 1.2		30.9 ± 0.5		**30.5 ± 0.6**
Otulum A.D. 600–700											
TC:10/98-4	11	180–500	0.86	0.87	19.8	4.3	38.7 ± 1.5	0.883	34.2 ± 1.3	(0.960)	34.2 ± 1.3
TC:10/98-5	13	100–500	0.84	0.87	32.4	1.7	45.0 ± 1.0	0.839	37.8 ± 0.8	(0.980)	37.8 ± 0.8
TC:10/98-6	12	100–470	0.88	0.87	15.5	4.6	38.2 ± 1.9	0.810	30.9 ± 1.5	(0.978)	30.9 ± 1.5
TC:5/93-4	11	180–500	0.86	0.85	30.4	2.5	39.4 ± 1.0	n.d.	n.d.	1.000	n.d.
TC:5/93-5	13	100–500	0.84	0.87	31.7	5.0	31.8 ± 0.7	0.911	29.0 ± 0.6	1.000	29.0 ± 0.6
TC:5/93-6	13	100–500	0.85	0.88	36.4	3.9	36.0 ± 0.7	0.900	32.4 ± 0.6	(0.996)	32.4 ± 0.6
TC:1/97-5	8	255–470	0.66	0.81	38.8	2.8	37.5 ± 0.5	0.816	30.6 ± 0.4	(0.965)	30.6 ± 0.4
TC:1/97-6	10	220–500	0.77	0.85	34.7	1.7	45.7 ± 0.9	0.734	33.5 ± 0.7	(0.986)	33.5 ± 0.7
TCF:26/93-3	8	100–355	0.68	0.83	30.9	2.8	29.8 ± 0.6	0.912	27.2 ± 0.5	1.043	26.1 ± 0.5
TCF:26/93-4	7	140–355	0.67	0.82	30.3	1.3	34.2 ± 0.6	0.916	31.3 ± 0.5	1.037	30.2 ± 0.5
TCF:26/93-5	13	100–500	0.90	0.90	14.2	5.4	33.4 ± 1.9	0.809	27.0 ± 1.5	1.013	26.7 ± 1.5
Unweighted average:							37.2 ± 1.5		31.4 ± 1.0		31.1 ± 1.1
Weighted average:							36.0 ± 1.6		30.9 ± 1.1		**30.5 ± 1.1**
Cascadas A.D. 500–600											
TC:65/92-2	13	190-500	0.76	0.90	24.5	6.3	32.4 ± 0.9	0.840	27.2 ± 0.8	1.009	27.0 ± 0.8

Table 1 (*continued*)

Sample	n	T °C (min–max)	f	g	q	DRAT (%)	H (μT)	$\mathcal{F}_{aTRM}$	H_{aTRM} (μT)	$\mathcal{F}_{CR}$	$H_{aTRM,CR}$ (μT)
TC:65/92-3	14	160-500	0.82	0.91	33.2	4.0	28.9 ± 0.7	1.050	30.3 ± 0.7	1.014	29.9 ± 0.7
TC:65/92-4	13	190-500	0.76	0.90	41.3	4.0	37.7 ± 0.6	0.819	30.9 ± 0.5	1.016	30.4 ± 0.5
TC:65/92-5	12	140-500	0.82	0.89	31.7	3.0	39.2 ± 0.9	0.947	37.1 ± 0.9	1.003	37.0 ± 0.9
TS:5/92-1	8	120-470	0.82	0.84	7.4	3.7	34.1 ± 3.2	0.998	34.0 ± 3.2	n.d.	n.d.
TS:5/92-2	17	20-500	0.88	0.92	27.5	3.1	31.4 ± 0.9	1.009	31.7 ± 0.9	1.012	31.3 ± 0.9
TS:5/92-3	16	100-500	0.84	0.92	65.5	2.3	40.8 ± 0.5	0.853	34.8 ± 0.4	1.000	34.8 ± 0.4
TS:5/92-4	16	100-500	0.85	0.91	60.0	1.9	31.5 ± 0.4	1.056	33.3 ± 0.4	1.015	32.8 ± 0.4
TS:5/92-5	12	100-470	0.79	0.90	18.3	2.2	31.4 ± 1.2	0.926	29.1 ± 1.1	1.034	28.1 ± 1.1
TS:4/93-2	10	140-440	0.71	0.88	15.7	7.0	44.1 ± 1.8	0.941	41.5 ± 1.7	1.024	40.5 ± 1.7
TS:4/93-3	13	100-500	0.81	0.90	41.5	1.7	42.5 ± 0.8	0.813	34.6 ± 0.7	1.006	34.3 ± 0.7
TS:4/93-4	13	100-500	0.85	0.90	21.1	2.7	38.6 ± 1.4	0.822	31.7 ± 1.2	1.027	30.9 ± 1.2
Unweighted average:							36.1 ± 1.5		32.9 ± 1.2		32.5 ± 1.2
Weighted average:							35.4 ± 1.5		32.8 ± 1.2		**32.5 ± 1.2**
Motiepa A.D. 400–500											
TC: Pasta 51-3	9	100-310	0.65	0.86	17.0	1.6	28.6 ± 0.9	1.005	28.7 ± 0.9	1.014	28.3 ± 0.9
TC: Pasta 51-4	13	100-400	0.78	0.91	41.8	3.0	29.5 ± 0.5	0.998	29.4 ± 0.5	1.018	28.9 ± 0.5
TC: Pasta 51-5	10	100-330	0.70	0.88	18.2	2.1	30.0 ± 1.0	1.070	32.1 ± 1.1	1.014	31.7 ± 1.1
TC: Pasta 51-6	9	100-380	0.73	0.84	20.9	6.9	30.8 ± 0.9	1.061	32.7 ± 1.0	1.052	31.1 ± 1.0
TC:51/92-2	13	100-500	0.81	0.90	9.9	4.6	44.3 ± 3.3	0.765	33.9 ± 2.5	1.045	32.4 ± 2.4
TC:51/92-3	7	140-355	0.51	0.83	4.2	9.5	33.8 ± 3.4	0.807	27.3 ± 2.7	1.088	25.1 ± 2.5
TC:51/92-4	10	100-400	0.65	0.86	5.6	7.3	36.9 ± 3.7	0.838	30.9 ± 3.1	1.068	28.9 ± 2.9
TC:51/92-5	10	180-470	0.77	0.88	7.8	3.3	37.4 ± 3.2	0.723	27.0 ± 2.3	1.065	25.4 ± 2.2
TC:51/92-6	9	140-400	0.68	0.87	8.2	5.6	27.2 ± 2.0	0.926	25.2 ± 1.9	1.090	23.1 ± 1.7
TC:1/89-2	14	20-400	0.83	0.90	11.8	6.1	36.3 ± 2.3	0.918	33.0 ± 2.1	1.086	30.7 ± 1.9
TC:1/89-3	9	100-310	0.54	0.83	12.3	9.9	41.0 ± 1.5	n.d.	n.d.	1.076	n.d.
TC:1/89-4	13	160-470	0.79	0.88	8.9	4.8	33.8 ± 2.7	0.843	28.5 ± 2.3	1.041	27.4 ± 2.2
TC:1/89-5	9	140-400	0.64	0.86	10.8	6.2	39.5 ± 2.0	0.902	35.6 ± 1.8	1.066	33.4 ± 1.7
TC:1/89-6	10	100-400	0.67	0.85	7.1	6.8	23.2 ± 1.9	1.115	25.9 ± 2.1	1.007	25.7 ± 2.1
Unweighted average:							33.7 ± 1.6		30.0 ± 0.9		28.6 ± 0.9
Weighted average:							30.7 ± 1.8		30.0 ± 0.9		**29.1 ± 0.9**

n is the number of points in the interval of temperature Tmin–Tmax used to determine the archeointensities; the fraction of NRM (f), the gap factor (g), and the quality factor (q) were calculated according to Coe et al. (1978); DRAT corresponds to the difference ratio between repeat pTRM steps normalized by the length of the selected NRM-pTRM segment; H is the uncorrected archeointensity estimate for individual specimen and uncertainty; $\mathcal{F}_{aTRM}$ and $\mathcal{F}_{CR}$ are the scaling factors for TRM anisotropy and cooling rate corrections, respectively; the weighted averages for uncorrected archeointensities H, ATRM corrected archeointensities H_{aTRM}, and ATRM plus cooling rate corrected archeointensities $H_{aTRM,CR}$ are calculated using $1/\sigma^2$ as the weighting parameters. Uncertainties around the estimate of the means are quoted with standard errors.

thermoremanent magnetization acquisition capacity. All heating–cooling cycles were performed in air. In our paleointensity furnace, the temperature reproducibility between heatings at the same step is within 1 °C, and the intensity of laboratory field is maintained with a precision better than 0.1 μT (Camps et al., 2011). After each heating–cooling cycle, the remanent magnetization was measured with a 2G cryogenic magnetometer.

4.2.1. Anisotropy correction

Archeomagnetic materials such as pottery, ceramics or bricks are often characterized by a strong magnetic anisotropy (e.g. Aitken et al., 1981; Veitch et al., 1984). So, the strength of the artificial TRM acquired in the laboratory is dependent on the direction along which the magnetic field is applied. Unless the magnetic field is applied along the direction of the ancient field, an error will be introduced in the determination of the archeointensity. The importance of this error depends directly on the degree of anisotropy of the sample and on the relative orientations of the ancient field and the laboratory field with respect to the principal anisotropy axes. In order to correct this bias, it is necessary to determine the anisotropic tensor for each sample. Chauvin et al. (2000) have shown that anisotropies of the magnetic susceptibility (A-MS), of the anhysteretic remanent magnetization (A-ARM), and of the thermo-remanent magnetization (A-TRM) present the same orientation of their principal axes but their shapes vary. We choose to correct our archeointensity measurements by means of the anisotropy of TRM. The A-TRM tensor (T) was determined at 290 °C. The samples were remagnetized at this temperature in $+X$, $-X$, $+Y$, $-Y$, $+Z$, and $-Z$ directions. All archeointensity values were corrected for the A-TRM according to Veitch et al.'s (1984) method, which first calculates the direction of the ancient field $\mathcal{H}_{anc}$ as

$$\mathcal{H}_{anc} = \frac{T^{-1} \cdot M_{ChRM}}{|T^{-1} \cdot M_{ChRM}|} \quad (1)$$

where M_{ChRM} is the direction of the characteristic magnetization in a sample coordinate obtained from the paleointensity determination. The scaling factors for TRM anisotropy correction is given by

$$\mathcal{F}_{aTRM} = \frac{|T \cdot \mathcal{H}_{lab}|}{|T \cdot \mathcal{H}_{anc}|} \quad (2)$$

where $\mathcal{H}_{lab}$ is the laboratory field applied along the core z-axis. Then, the A-TRM corrected archeointensity H_{aTRM} is given by

$$H_{aTRM} = \mathcal{F}_{aTRM} \cdot H \quad (3)$$

where H is the uncorrected archeointensity.

4.2.2. Cooling rate correction

The effect of the cooling rate (CR) on the acquisition of a TRM was first reported by Néel (1955) and later by Dodson and McClelland (1980) and Walton (1980), before to be applied to archeomagnetism (e.g. McClelland-Brown, 1984). For baked clays carrying single domain magnetic grains, the TRM acquired during a fast cooling as occurred during laboratory experiments is lower than the one acquired during a slow cooling as occurring in archeological furnaces. The effect of the CR on our samples was evaluated using the experimental procedure of Chauvin et al. (2000). First, two heating–cooling cycles were performed at the temperature of 220 °C using a slow and a fast cooling rate: TRM_1 is the TRM acquired during a fast cooling (3 h) and TRM_2 is the TRM acquired during a slow cooling (12 h). The effect of the cooling rate was calculated by the ratio $\mathcal{F}_{CR}$ defined as

$$\mathcal{F}_{CR} = \frac{TRM_2}{TRM_1} \quad (4)$$

Then a third TRM, TRM_3, was acquired by the samples by means of the same procedure as the initial one, using a same cooling rate. Changes in the TRM acquisition of the samples were evaluated by the ratio $\mathcal{F}_{CR2}$ defined as

$$\mathcal{F}_{CR2} = \frac{TRM_3}{TRM_1} \quad (5)$$

which quantifies the alteration of the magnetic carrier properties. For each sample, we compared both factors. The CR correction was considered significant and thus applicable only if $\mathcal{F}_{CR} > 1$ and if the ratio $\mathcal{F}_{CR2}$ was close to 1 or lower than $\mathcal{F}_{CR}$. The corrected archeointensity is given by

$$H_{aTRM,CR} = \frac{H_{aTRM}}{\mathcal{F}_{CR}} \quad (6)$$

4.3. Archeointensity results

Archeointensity data were interpreted by means of the Thellier-tool software provided by Leonhardt et al. (2004). We adopted a standard set of criteria derived from those of Selkin and Tauxe (2000) and based on the statistical parameters introduced by Coe et al. (1978) and modified by Prévot et al. (1985) in order to interpret each individual archeointensity data and filter out those of poor technical quality

1. Archeointensity measurements are represented with Arai's diagram in which the NRM left is plotted against the pTRM acquired after each heating step. The slope of the least-squares-fit line computed from the linear part of the diagram gives an estimate of the archeointensity. A value is accepted when the linear segment is defined by more than four points ($n > 4$) and spans over 30% of the total extrapolated ChRM ($f > 0.3$).
2. pTRM checks estimate the thermal alteration of magnetic properties for each sample and assess the reliability of the archeointensity. We quantified the difference between two pTRM acquisitions at the same temperature step with the Difference Ratio (DRAT) parameter (Selkin and Tauxe, 2000). DRAT corresponds to the maximum difference measured in percent between two repeated pTRM acquisition normalized by the length of the selected NRM-TRM segment. We fixed arbitrarily a maximum acceptable DRAT of 10%.
3. Finally, we checked on the Zijderveld plots computed from the archeointensity measurements that the NRM fraction used to calculate the archeointensity may correspond to the ChRM, or at least to a part of the whole ChRM. The low-temperature part of the NRM may contain natural secondary magnetizations, and at high temperature a chemical remanent magnetization may be acquired during the laboratory heating. This check is performed qualitatively by a visual inspection of the vector endpoint diagrams. The points in the selected interval should trend toward the origin if the NRM is the ChRM.

All archeointensity determinations are gathered in Table 1 and a qualitative appreciation of the results is given for samples from two hollow flanged pedestals in Supplementary Fig. S4. The scaling factors used to correct the measured paleointensities for the cooling rate ($\mathcal{F}_{CR}$) and anisotropy ($\mathcal{F}_{aTRM}$) effects are reported in Table 1. The corrections for cooling rate are rather small with a maximal correction of 9% (Table 1). On the contrary, the effect of anisotropy of TRM can be relatively important provided that $\mathcal{F}_{aTRM}$ are in the range of 0.743–1.115. Two points deserve to be noted on the importance of A-TRM correction on the final archeointensity results. First, in most cases the corrected archeointensity value is lower than the uncorrected one. Second,

uncertainties around the estimate of the means are always lower after than before A-TRM corrections, which is *a posteriori* a good justification to apply this correction. In total, we obtained a high success rate, with 19 mean archeointensities determined from the 24 hollow flanged pedestals and with 9–19 samples per ceramic period.

5. Archeological firing conditions

Identifications of firing conditions of the flanged clay pedestals are important to validate our archeointensity measurements. To get insight into manufacturing firing conditions, we analyzed three representative samples (Pasta −51, TC-65/92 and TC-41/92) by means of X-Ray Powder Diffraction (XRPD) and Mössbauer spectroscopy.

5.1. X-ray powder diffraction

The presence or absence of specific mineral assemblages determines the degree of thermal transformation which has occurred in the clay paste of ceramics during the firing. As a consequence the firing temperature during the procedure can be estimated by means of XRPD, revealing either the presence of primary minerals representative of their raw materials or the crystallization of new high-temperature minerals resulting from reactions between the decomposed primary minerals as the temperature raises (e.g. Rathossi et al., 2011, and references herein). A multichannel high-performance sequential Wavelength Dispersive X-Ray Fluorescence (WDXRF) spectrometer (Axios 2005, PANalytical, Netherlands) was used. The WDXRF allowed rapid and accurate elemental analysis. The X-ray tube in the present WDXRF spectrometer had Rh anode and operated at a maximum power of 4 kW and a maximum current of 160 mA. For each sample, the characteristic radiation of the major, minor and trace elements were recorded under vacuum in 14 different scans. Each scan covers a certain number of the expected elements and the peak areas of the characteristic radiation were measured. Gas proportional (Ar/CH_4) and scintillation counters were used for recording the intensities of characteristic radiations. Visual inspection of samples permits to distinguish quartz grains that have been removed prior to XRPD analyses. Despite this precaution, powder diffraction patterns of the samples reveal that the main crystallized phase remains unambiguously quartz (Supplementary Fig. S2). The diffraction peaks not belonging to quartz are generally broadened or of very low intensity making difficult their reliable assignment. The absence of primary clay minerals such as illite, smectite or calcite or few remains of muscovite and the presence of high-T new phases such as K-feldspar or anorthite are arguments in favor of a firing temperature minimum to 700 °C (Cultrone et al., 2001; Maritan et al., 2006).

5.2. Mössbauer spectroscopy

Several parameters retrieved from Mössbauer spectroscopy such as the value of the quadrupole splitting or the relative amount of magnetic and non-magnetic iron can give a clear indication on the redox conditions and the firing temperature used in ceramics manufacturing (Murad and Wagner, 1989, 1998; Wagner et al., 1998; Ricciardi et al., 2008). Hence, we measured Mössbauer spectra at room temperature (Supplementary Fig. S3a–c) in order to get better insight into the nature of iron existing in the studied samples, and thus to check the conclusion on the firing temperatures drawn from the XRPD analyses. The spectra were recorded in the transmission geometry with a constant-acceleration spectrometer which utilized a rhodium matrix ^{57}Co source calibrated at

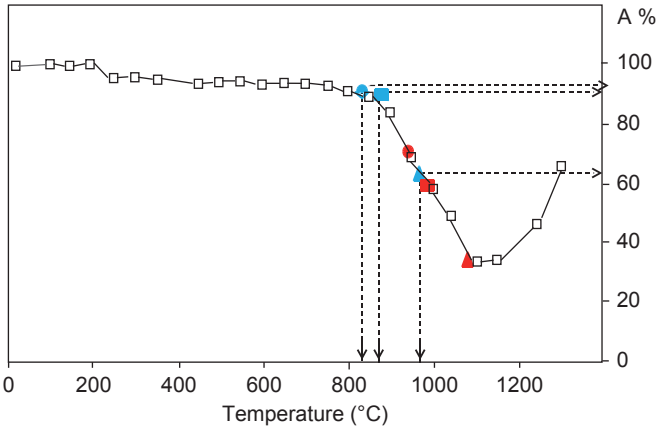

Fig. 5. Estimated firing temperature based on the non-magnetic iron (right axis). Figure adapted from Murad and Wagner (1989). Pasta 51: triangle, TC-65/92: squares and TC-41/92: circles. Blue (red) symbols are measurements before (after) laboratory firing. (For interpretation of the references to color in this figure legend, the reader is referred to the web version of this article.)

295 K with α-iron foil. The obtained data indicate that all the samples contain iron in the magnetic and non-magnetic states. The samples differ by the relative amount of iron in magnetically ordered state (40, 20 and 15% for samples Pasta −51, TC-65/92 and TC-41/92, respectively). The best fit of the spectrum is obtained by considering two doublets for the non-magnetically ordered iron and two sextets ordered. The non-magnetic iron is in the ferric state with a wide distribution of sites symmetries since the quadrupole splitting varies from 0.7 to 1.6 mm/s. The two sextets indicate the presence of magnetite and probably some maghemite (Dyar et al., 2006). In this case one can conclude that paramagnetic iron is mainly Fe^{3+} in octahedral environments with more or less distorted sites. Concerning the magnetic part, the values of the hyperfine field (45–52 T) suggest the presence of phases such as magnetite, hematite and maghemite (McCammon, 1995). The value of the quadrupole splitting is more model-dependent than the amount of magnetic and non-magnetic iron. Thus, because we do not have the raw clay ceramic composition, we decided to use the non-magnetic iron fraction parameter (A_{nm}) for the estimation of the firing temperatures, i.e., the relative area of all components in the Mössbauer spectra that do not exhibit a magnetic hyperfine splitting (Murad and Wagner, 1989). Assuming that A_{nm} is weakly dependent on the raw clay ceramic composition, the comparison of our data with those reported by Murad and Wagner (1989) for Peruvian clays yields estimates of the initial firing temperatures around 980 °C for sample Pasta-51, and between, let say, 400 and 850 °C for samples TC-41-92 and TC-65/92 (Fig. 5). This large interval reduces to a smaller one, 700–850 °C, if we take into account the conclusions reached with the XRPD analyses.

5.3. Firing experiments

In order to check the firing temperature estimations, samples were fired at 1100 °C for 10 h under air to compare changes occurring in the mineralogy. After heating, the samples showed similar colors. The XRD patterns and Mössbauer spectra are given in Supplementary Figs. S2 and S3d–f. As for the original samples, the patterns of the fired samples are mainly composed of quartz. Very slight modifications are observed; hematite appeared at the expense of many minor peaks that have disappeared after firing. Mössbauer data show an increase in the magnetic ordered part for all the samples. In the same time, one of the non-magnetic doublets decreases significantly indicating that firing induces the transformation of non-magnetic phases to magnetic ones.

Replacing our new values for A_{nm} in Fig. 5, we estimated the new firing temperature between 1000 °C and 1100 °C that corresponds to the laboratory heating temperature. Thus, we conclude that our first estimation of the firing temperatures was quite accurate and that Mayan ceramics were fired in kilns where the temperature was comprised between 700 °C and 1000 °C.

6. Discussion

6.1. Reliability of the archeointensity determinations

The overall technical quality of the present archeointensities is very good as attested by the quality factors ranging from 6.9 to 80.8. We observed well-defined straight segments on NRM–TRM curves over a large range of NRM fraction; 66% of the archeointensity estimates are calculated with a NRM fraction greater than 40%. In addition, the individual archeointensity estimates are fairly coherent when they are compared within a single ceramic phase. This is particularly true after the cooling rate and the TRM anisotropy corrections. We calculated a weighted mean and a standard error about the mean for each phase, using the weighting by the reciprocal of variance of individual determinations. Each mean ceramic phase intensity value was calculated with at least nine samples and presents a very low standard error smaller than 4% about the mean. The X-ray diffraction results and Mössbauer spectra yield additional arguments to validate our archeointensity determinations. These experiments, which are independent of magnetic remanence properties, concluded for very high firing temperatures during the manufacturing process. Indeed, the initial firing temperatures for all the incense burners, estimated between 850 °C and 1000 °C, are sufficiently high to ensure the formation of magnetic minerals and to record during cooling a full TRM. Thus, we believe this new dataset to be very reliable.

6.2. Archeomagnetic evidence for the Motiepa phase

According to these results, the magnetic field intensity varied slightly during the Classic period in Mesoamerica, from a minimum of 29.1 ± 0.9 μT during Motiepa to a maximum of 32.5 ± 1.2 μT during Cascadas. This corresponds to a virtual axial dipole moment (VADM) varying from $6.7 \pm 0.2 \times 10^{22}$ A.m^2 to maximum $7.4 \pm 0.3 \times 10^{22}$ A.m^2 during these four centuries. These new archeointensities are important for archeometry because they could help to clarify the different ceramic phases. In particular, they could confirm the chronology of incense burners before the Murcielagos phase since the presence of objects associated with Motiepa and Cascadas do not present any hieroglyphic inscriptions in the archeological complex of the Cross. Although Cascadas subdivisions have been removed from the Motiepa phase (Rands, 2007) and that they do not appear in all seriations of the incense burners, it would seem that two stages could be distinguished during Motiepa phase according to several authors (Román, 2005; Cuevas-García, 2007). Indeed, incense burners from 400 to 600 A.D. do not form a homogeneous group as they present variations in manufacturing techniques, iconic designs and styles. Such differences may be attributed to their development at different times within this period of 200 years. Our study, based on the seriation proposed by Cuevas-García (2007), seems to confirm two subdivisions: early Motiepa and late Motiepa (Cascadas) phases since a difference in the mean field intensity is observed; 29.1 ± 0.9 μT and 32.5 ± 1.2 μT during early Motiepa and Cascadas, respectively. A two-sample Student's *t*-test assuming equal variances using a pooled estimate of the variance was performed to ascertain whether the mean archeointensity for Motiepa and Cascadas are statistically different. In this test the null hypothesis that the two means are the same ($H_0 : \mu_1 = \mu_2$) is checked against the alternative hypothesis that the two means are different ($H_a : \mu_1 \neq \mu_2$). There is statistical evidence from our measurements against the null hypothesis, $t(22) = 2.6299$, $p = 0.0153 < 5\%$, calculated with a pooled standard deviation $SD = 3.5562$. In other words, we can argue in favor of a subdivision of the Motiepa phase into an early Motiepa phase (400–500 A.D.) and a Cascadas phase (500–600 A.D.).

6.3. Comparison with previous data in Mesoamerica and global models

We gathered all archeointensity data encompassing the last three millennia that have been obtained in Mesoamerica from archeologic artifacts or basalts, by means of all methodologies (Thellier–Thellier type, Shaw, microwave or multispecimen methods). This was achieved by a simple query to the GEOMAGIA database[1] (Donadini et al., 2006; Korhonen et al., 2008) with geographical constraints similar to the ones used to plot Fig. 6. In total, 98 archeointensity determinations are available for this area and this time interval. A first point regarding our compilation need a comment: the abundance of archeological material in Mesoamerica contrasts with the small amount of sites that have been investigated for archeointensity studies as illustrated in Fig. 6. This observation is even more important that a first selection is required. It was achieved by keeping only data from sites located within a 900 km radius circle centered at Palenque. Doing thus, we want to avoid a scattering in the experimental data induced by possible regional anomalies of the geomagnetic field. The confrontation of the data to the global models give also reasons for such selection since the modeling outcomes remain more or less constant within such area and differ sensibly when apply to remote sites located beyond this area. The 58 remaining experimental data are very scattered as illustrated in Fig. 7a. This large dispersion reveals obviously some undetected experimental problems during the data acquisition process. Honestly, it is very complicated to assess the reliability of data included in database because sources of errors are numerous. The scatter pattern of data could be explained either by the methodology, by the absence of cooling rate correction and/or anisotropy correction on data obtained from archeological artifacts, or by biased estimates of ages. For example, the Shaw (1974) method is not a conventional method in paleo- and archeointensity determinations and can yield significant over- or underestimations of the ancient intensity. Thus, we decided to select only measurements satisfying the following conditions:

1. The data must be obtained by means of Thellier-like methods or the recent MultiSpecimen protocol as proposed by Dekkers and Böhnel (2006).
2. If the data was carried out from an archeological artifact, A-TRM and CR corrections should have been applied.
3. An alteration control by means of pTRM checks must have been performed during the experiment.

Even with this very gentle set of selection criterium, almost all the data are rejected, only 13 were kept (Fig. 7a). Their dispersion remains surprisingly important maintaining some doubts on their reliability. As a consequence, our new data cannot be compared to the previously published data obtained from sites located in the regional vicinity of Palenque. Despite the study of several sites and periods in the last decade, a regional secular variation curve cannot be built. In this context, our high technical quality data represent a strong constraint for the Mesoamerican secular variation curve and

[1] Available at: https://geomagia.ucsd.edu.

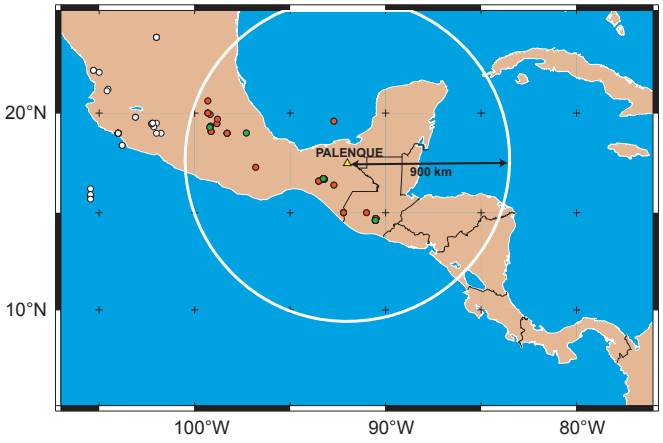

Fig. 6. Geographical distribution of the sites in Mesoamerica that yield archeointensity data whose age is in the range 1000 BC–2000 A.D. Only data from sites located within a 900 km radius circle centered at Palenque were kept in the present analysis. Within this circle, the sites yielding archeointensity measurements satisfying our set of quality criterium (see text) are plotted in green, the others in red. (For interpretation of the references to color in this figure legend, the reader is referred to the web version of this article.)

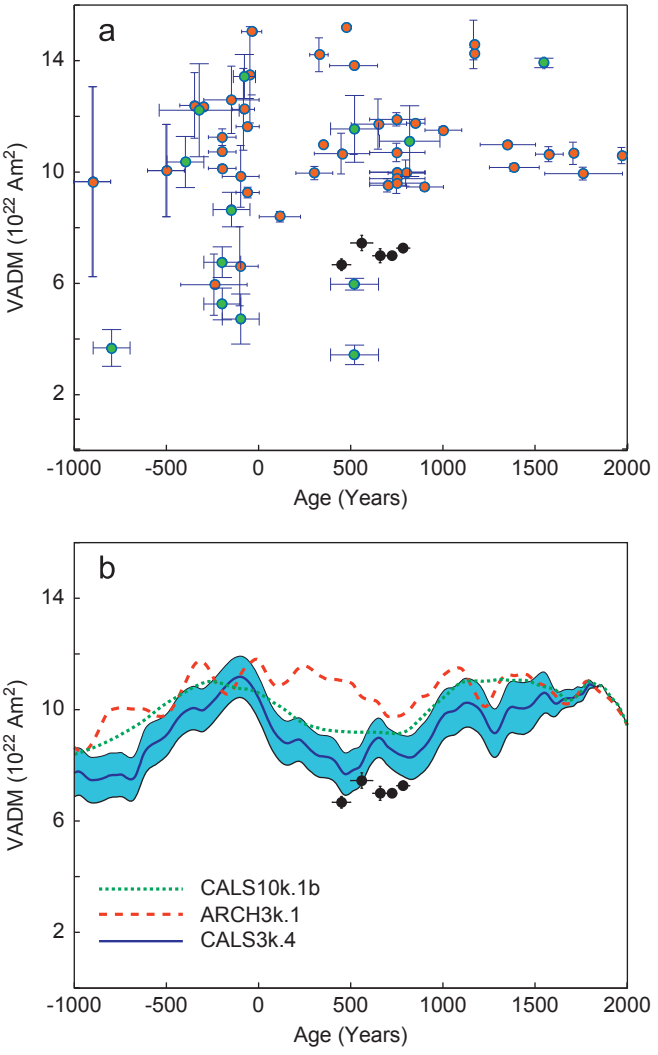

Fig. 7. Compilation of archeointensity VADM data selected for Mesoamerica as explained in the text and Fig. 6. (a) All selected data of good (poor) technical quality are plotted in green (red) altogether with the present study data (black circles). (b) Confrontation of our Palenque VADM with the CALS3k.4 global model (blue line) represented with its 95% confidence interval (shaded area). The models CALS10k.1b (green dotted line) and ARCH3.1 (red dashed line) are also represented. (For interpretation of the references to color in this figure legend, the reader is referred to the web version of this article.)

global models. The confrontation of our new data with the global model CALS3k.4 (Korte and Constable, 2011) calculated for Palenque location seems to validate further their reliability (Fig. 7b). Our low VDM values correspond to a minimum value predicted by this model. We can however easily imagine that this global model is poorly constrained for Palenque area due to the large dispersion observed in the existing data. The global models ARCH3k (Donadini et al., 2009) and CALS10k (Korte et al., 2011) are also plotted. If they are true, our data would confirm that the ARCH3k model is not applicable for region outside Europe since it was built only from european data, and that the CALS10k.1 model is too smooth to predict accurately the fluctuation in the secular variation at a scale of few hundred years.

The present study show unambiguously that more data from the maya area are required, in particular to confirm the low VADM values found between 400 and 850 A.D. Calakmul was one of the two most important Maya cities in the Classic period. Located in the center of the Yucatan peninsula (Fig. 1) this site appears as the ideal candidate for a next study. Larger numbers of high-quality data will allow the rejection of data of unknown or questionable quality, improving the signal-to-noise ratio in the global and regional datasets. This step is of first importance to increase global model resolution both in space and time resolution to answer questions of geophysical interests and to enable the development of reliable regional reference curves involved in archeomagnetic dating.

7. Conclusions

Of the 24 samples from Mayan incense burners used to estimate the archeointensity during the Classic period at Palenque, 19 yield a reliable determination. Measurements were performed with Thellier–Thellier's method on pre-selected samples by means of their magnetic properties. We estimated the firing temperature of the ceramics between 700 °C and 1000 °C that ensures that a full thermoremanent magnetization was acquired during the manufacturing heating. The present experimental study leads to the following conclusions:

1. The intensity of the Earth's magnetic field varied slightly during the Classic Maya period, from a minimum of 29.1 ± 0.9 μT during Motiepa to a maximum of 32.5 ± 1.2 μT during Cascadas. This corresponds to a virtual axial dipole moment (VADM) varying from a minimum of $6.7 \pm 0.2 \times 10^{22}$ A.m^2 to a maximum of $7.4 \pm 0.3 \times 10^{22}$ A.m^2.
2. These new archeointensities help to clarify the different ceramic phases. Indeed, incense burners from 400 to 600 A.D. do not form a homogeneous group as they present variations in manufacturing techniques, iconic designs and styles. Such differences may be attributed to the development at different times within this period of 200 years. Our study clearly argues in favor for a subdivision of the Motiepa phase into an early Motiepa phase (400–500 A.D.) and a Cascadas phase (500–600 A.D.).
3. The abundance of archeological material in this region contrasts with the small amount of archeomagnetic data in Mesoamerica available over the last few millennia. Moreover, these data are also of uneven quality. Thus, it is especially difficult to establish a trend in the intensity variations in the Mesoamerican region, even using the global databases and predictions of secular variation of the existing global models.

As a consequence, our high technical quality data represent a strong constrain in the Mesoamerican secular variation curve. The VADM values found are substantially smaller than the ones predicted by the global geomagnetic model CALS3k.4, suggesting the need to develop a regional model for the secular variation curve in Mesoamerica.

Acknowledgments

We are grateful to Thierry Poidras and Patrick Nicol for technical help during the laboratory experiments. Sylvie Raynaud provided valuable references. This project was supported by grants to Géosciences Montpellier from the CNRS-PNP and INSU-PICS#5319 programs and by grants to Instituto de Geofísica (UNAM) from PAPIIT-UNAM IN108711 and CONACYT 105194 research projects.

Appendix A. Supporting information

Supplementary data associated with this article can be found in the online version at http://dx.doi.org/10.1016/j.epsl.2012.12.035.

References

Aidona, E., Kondopoulou, D., 2012. First archaeomagnetic results and dating of Neolithic structures in Northern Greece. Stud. Geophys. Geod. 56, http://dx.doi.org/10.1007/s11200-011-9006-8.

Aitken, M.J., Alcock, P.A., Bussell, G.D., Shaw, C.J., 1981. Archeomagnetic determination of the past geomagnetic intensity using ancient ceramics: allowance for anisotropy. Archeometry 23, 53–64.

Alva-Valdivia, L., 2005. Comprehensive paleomagnetic study of a succession of Holocene olivine-basalt flow: Xitle Volcano (Mexico) revisited. Earth Planets Space 57, 839–853.

Alva-Valdivia, L., Morales, J., Goguitchaichvili, A., de Hatch, M.P., Hernandez-Bernal, M., Mariano-Matias, F., 2010. Absolute geomagnetic intensity data from preclassic Guatemalan pottery. Phys. Earth Planet. Inter. 180, 41–51.

Bishop, R., Rands, R., Harbottle, G., 1982. A ceramic compositional interpretation of incense burner trade in the palenque area, Mexico. In: Currie, L. (Ed.), Nuclear and Chemical Dating Techniques. American Chemical Society, Washington, DC, pp. 411–440.

Bucha, V., Taylor, R., Berger, R., Haury, E., 1970. Geomagnetic intensity: changes during the past 3000 years in the western hemisphere. Science 168, 111–114.

Camps, P., Prévot, M., 1996. A statistical model of the fluctuations in the geomagnetic field from paleosecular variation to reversal. Science 273, 776–779.

Camps, P., Singers, B., Carvallo, C., Goguitchaichvili, A., Fanjat, G., Allen, B., 2011. The Kamikatsura event and the Matuyama–Brunhes reversal recorded in lavas from Tjornes peninsula, northern Iceland. Earth Planet. Sci. Lett. 310, 33–44.

Ceja, M.R., Goguitchaichvili, A., Morales, J., Ostroumov, M., Manzanilla, L.R., Aguilar-Reyes, B., Urrutia-Fucugauchi, J., 2009. Integrated archeomagnetic and micro-Raman spectroscopy study of pre-Columbian ceramics from the Mesoamerican formative village of Cuanalan, Teotihuacan Valley, Mexico. J. Geophys. Res. 114, http://dx.doi.org/10.1029/2008JB006106.

Chauvin, A., Garcia, Y., Lanos, P., Laubenheimer, F., 2000. Paleointensity of the geomagnetic field recovered on archaeomagnetic sites from France. Phys. Earth Planet. Inter. 120, 111–136.

Coe, R.S., Grommé, S., Mankinen, A., 1978. Geomagnetic paleointensities from radiocarbon-dated lava flows on Hawai and the question of the Pacific nondipole low. J. Geophys. Res. 83, 1740–1756.

Conte-Fasano, G., Urrutia-Fucugauchi, J., Goguitchaichvili, A., Morales, J., 2006. Low-latitude paleosecular variation and the time-averaged field during the late pliocene and quaternary paleomagnetic study of the Michoacan-Guanajuato volcanic field, Central Mexico. Earth Planets Space 58, 1359–1371.

Cuevas-García, M., 2007. Los incensarios efigie de Palenque: Deidades y rituales mayas. Universidad Nacional Autónoma de México, Instituto de Investigaciones Filológicas.

Cultrone, G., Sebastian, E., Rodríguez-Navarro, C., Cazalla, O., De La Torre, M.J., 2001. Carbonate and silicate phase reactions during ceramic firing. Eur. J. Mineral. 13, 621–634.

Day, R., Fuller, M., Schmidt, V.A., 1977. Magnetic hysteresis properties of synthetic titanomagnetite. Phys. Earth Planet. Inter. 15, 260–266.

Dekkers, M.J., Böhnel, H.N., 2006. Reliable absolute paleointensities independant of magnetic domain state. Earth Planet. Sci. Lett. 248, 508–517.

Dodson, M.H., McClelland, E., 1980. Magnetic blocking temperatures of simple domain grains during slow cooling. J. Geophys. Res. 85, 2625–2637.

Donadini, F., Korhonen, K., Riisager, P., Pesonen, L., 2006. Database for holocene geomagnetic intensity information. EOS Trans. Am. Geophys. Union 87 (14), 137.

Donadini, F., Korte, M., Constable, C., 2009. Geomagnetic field for 0–3 ka: 1. New data sets for global modeling. Geochem. Geophys. Geosyst. 10 (6), Q06007, http://dx.doi.org/10.1029/2008GC002295.

Donadini, F., Korte, M., Constable, C., 2010. Millennial variations of the geomagnetic field: from data recovery to field reconstruction. Space Sci. Rev. 155, 219–246.

Dyar, M., Agresti, D., Schaefer, M., Grant, C., Sklute, E., 2006. Mössbauer spectroscopy of earth and planetary materials. Annu. Rev. Earth Planet. Sci. 34, 83–125.

Gallet, Y., Genevey, A., Goff, M.L., Warm, N., Gran-Aymerich, J., Lefévre, A., 2009. On the use of archeology in geomagnetism, and vice-versa: recent developments in archeomagnetism. C. R. Phys. 10, 630–648.

Gallet, Y., Genevey, A., LeGoff, M., 2002. Three millennia of directional variation of the Earth's magnetic field in western Europe as revealed by archeological artefacts. Phys. Earth Planet. Inter. 131, 81–89.

Genevey, A., Gallet, Y., Constable, C.G., Korte, M., Hulot, G., 2008. Archeoint an upgraded compilation of geomagnetic field intensity data for the past ten millennia and its application to the recovery of the past dipole moment. Geochem. Geophys. Geosyst. 9, http://dx.doi.org/10.1029/2007GC001881.

Gonzalez, S., Sherwood, G., Böhnel, H., Schnepp, E., 1997. Palaeosecular variation in central Mexico over the last 30 000 years; the record from lavas. Geophys. J. Int. 130, 201–219.

Hoffman, K., Singer, B., Camps, P., Hansen, L., Johnson, K., Clipperton, S., Carvallo, C., 2008. Stability of mantle control over dynamo flux since the mid-cenozoic. Phys. Earth Planet. Inter. 169 (1–4), 20–27.

Hongre, L., Hulot, G., Khokhlov, A., 1998. An analysis of the geomagnetic field over the past 2000 years. Phys. Earth Planet. Inter. 106 (3–4), 311–335.

Korhonen, K., Donadini, F., Riisager, P., Pesonen, L.J., 2008. GEOMAGIA50: an archeointensity database with PHP and MySQL. Geochem. Geophys. Geosyst. 9, Q04029, http://dx.doi.org/10.1029/2007GC001893.

Korte, M., Constable, C.G., 2011. Improving geomagnetic field reconstructions for 0–3 ka. Phys. Earth Planet. Inter. 188, 247–259.

Korte, M., Constable, C.G., Donadini, F., Holme, R., 2011. Reconstructing the holocene geomagnetic field. Earth Planet. Sci. Lett. 312, 497–505.

Kovacheva, M., Boyadziev, Y., Kostadinova-Aramova, M., Jordanova, N., Donadini, F., 2009. Updated archeomagnetic data set of the past 8 millennia from the Sofia laboratory, Bulgaria. Geochem. Geophys. Geosyst. 10, http://dx.doi.org/10.1029/2008GC002347.

Kovacheva, M., Jordanova, I.H.N., Kostadinova, M., Gigov, V., 2004. Archaeomagnetic dating of archaeological sites from Switzerland and Bulgaria. J. Archeol. Sci. 31, 1463–1479.

Lanos, P., LeGoff, M., Kovacheva, M., Schnepp, E., 2005. Hierarchical modelling of archaeomagnetic data and curve estimation by moving average technique. Geophys. J. Int. 160, 1440–1476.

Leonhardt, R., Heunemann, C., Krása, D., 2004. Analyzing absolute paleointensity determinations: acceptance criteria and the software ThellierTool4.0. Geochem. Geophys. Geosyst. 5, Q12016, http://dx.doi.org/10.1029/2004GC000807.

Lifton, N., Smart, D., Shea, M., 2008. Scaling time-integrated in situ cosmogenic nuclide production rates using a continuous geomagnetic model. Earth Planet. Sci. Lett. 268, 90–201.

López-Téllez, J., Aguilar-Reyes, B., Morales, J., Goguitchaichvili, A., Calvo-Rathert, M., Urrutia-Fucugauchi, J., 2008. Magnetic characteristics and archeointensity determination on Mesoamerican Pre-Columbian pottery from Quiahuiztlan, Veracruz, Mexico. Geofis. Int. 47 (4), 329–340.

Maritan, L., Nodari, L., Mazzoli, C., Milano, A., Russo, U., 2006. Influence of firing conditions on ceramic products: experimental study on clay rich in organic matter. Appl. Clay Sci. 31, 1–15.

McCammon, C.A., 1995. Mössbauer spectroscopy of minerals. In: Mineral Physics and Crystallography. Washington, DC, American Geophysical Union.

McClelland-Brown, E., 1984. Experiments on TRM intensity dependence on cooling rate. J. Geophys. Res. Lett. 11, 205–208.

Morales, J., Goguitchaichvili, A., Acosta, G., González-Moran, T., Alva-Valdivia, L., Robles-Camacho, J., Hernández-Bernal, M., 2009. Magnetic properties and archeointensity determination on Pre-Columbian pottery from Chiapas, Mesoamerica. Earth Planets Space 61, 83–91.

Morales, J., Goguitchaichvili, A., Urrutia-Fucugauchi, J., 2001. A rock magnetic and paleointensity study of some Mexican volcanic lava flows during the latest Pleistocene to the Holocene. Earth Planets Space 53, 893–902.

Murad, E., Wagner, U., 1989. Pure and impure clays and their firing products. Hyperfine Interact. 45, 161–177.

Murad, E., Wagner, U., 1998. Clays and clay minerals: the firing process. Hyperfine Interact. 117, 337–356.

Nagata, T., Kobayashi, K., Schwarz, E., 1965. Archaeomagnetic intensity studies of south and central America. J. Geomagn. Geoelectr. 17, 399–405.

Néel, L., 1955. Some theoretical aspects in rock magnetism. Adv. Phys., 191–243.

Nilsson, A., Snowball, I., Muscheler, R., Bertacchi-Uvo, C., 2010. Holocene geocentric dipole tilt model constrained by sedimentary paleomagnetic data. Geochem. Geophys. Geosyst. 11, Q08018.

Pavón-Carrasco, F., Rodríguez-González, J., Osete, M., Torta, J., 2011. A Matlab tool for archaeomagnetic dating. J. Archaeol. Sci. 38 (2), 408–419.

Pineda-Durán, M., Goguitchaichvili, A., Morales, J., Aguilar-Reyes, B., Alva-Valdivia, L.M., Oliveros-Morales, A., Calvo-Rathert, M., Gonzalez-Moran, T., Robles-Camacho, J., 2010. Magnetic properties and archeointensity of Earth's magnetic field recovered from El Opeño, earliest funeral architecture known in western Mesoamerica. Stud. Geophys. Geod. 54, 575–593.

Pineda-Durán, M., Morales, J., Aguilar-Reyes, B., Goguitchaichvili, A., 2011. Determinacion de arqueointensidades sobre vestigios de cerámica del sitio arqueólogico de Capacha (occidente de Mexico): en busca de afinidad con otras culturas mesoamericanas. Latinmag Lett. 1 (Special Issue), 1–5.

Prévot, M., Mankinen, E.A., Coe, R.S., Grommé, C., 1985. The Steens mountain (Oregon) geomagnetic polarity transition 2. Field intensity variations and discussion on reversal models. J. Geophys. Res. 90, 10417–10448.

Rands, R., 1974. A chronological framework for palenque. In: Greene-Robertson, M., Stevenson, R. (Eds.), Primera Mesa Redonda de Palenque, Part I. Available online at: 〈http://www.mesoweb.com/pari/publications/RT01/Chronological.html〉, p. 6.

Rands, R., 2007. Chronological chart and overview of development of ceramics at Palenque. In: Marken, D. (Ed.), Palenque: recent investigations at the classic Maya center. AltaMira Press, pp. 17–27.

Rands, R., Bishop, R., Harbottel, G., 1979. Thematic and compositional variation in palenque-region incensarios. In: Greene-Robertson, M., Call-Jeffers, D. (Eds.), Tercera Mesa Redonda de Palenque. Available online at: 〈http://www.mesoweb.com/pari/publications/RT04/Incensarios.html〉, p. 15.

Rathossi, C., Tsolis-Katagas, P., Katagas, C., 2011. Thermal behaviour of "Metamorphic Vermiculite" in Ca-rich ancient ceramic sherds and experimental ceramics. Mineral. Mag. 74 (4), 747–771.

Ricciardi, P., Nodari, L., Gualtieri, S., DeSimone, D., Fabbri, B., Russo, U., 2008. Firing techniques of black slipped pottery from Nepal (12th-3rd century BC): the role of Mössbauer spectroscopy. J. Cult. Herit. 9 (3), 261–268.

Rice, P.M., 1999. Rethinking classic lowland Maya pottery censers. Ancient Mesoamer. 10 (1), 25–50.

Román, M.E.S., 2005. El Clássico Temprano en Palenque a tráves de su cerámica. Lakamhá Museo de sitio y zona Arqueologica de Palenque, Chiapas, Mexico, pp. 3–8.

Selkin, P., Tauxe, L., 2000. Long term variations in palaeointensity. Philos. Trans. R. Soc. A: Math. Phys. Eng. Sci. 358 (1768), 1065–1088.

Shaw, J., 1974. A new method of determining the magnitude of the paleomanetic field application to five historic lavas and five archeological samples. Geophys. J. R. Astr. Soc. 99, 133–141.

Tema, E., Goguitchaichvili, A., Camps, P., 2010. Archaeointensity determinations from Italy: new data and the Earth's magnetic field strength variation over the past three millennia. Geophys. J. Int. 180, 596–608.

Tema, E., Kondopoulou, D., 2011. Secular variation of the Earth's magnetic field in the Balkan region during the last eight millennia based on archaeomagnetic data. Geophys. J. Int. 186, 603–614.

Thellier, E., Thellier, O., 1959. Sur l'intensité du champ magnétique terrestre dans le passé historique et géologique. Ann. Géophys. 15, 285–376.

Valet, J.-P., Herrero-Bervera, E., LeMouël, J.-L., Plenier, G., 2008. Secular variation of the geomagnetic dipole during the past 2000 years. Geochem. Geophys. Geosyst. 9, 1525–2027.

Veitch, R.J., Hedley, I.G., Wagner, J.J., 1984. An investigation of the intensity of the geomagnetic field during roman times using magnetically anisotropic bricks and tiles. Arch. Sc. Genève 37, 359–373.

Wagner, U., Gebhard, R., Grosse, G., Hutzelmann, T., Murad, E., Riederer, J., Shimada, I., Wagner, F., 1998. Clay: an important raw material for prehistoric man. Hyperfine Interact. 117, 323–335.

Walton, D., 1980. Time–temperature relations in the magnetization of assemblies of single domain grains. Nature 286, 245–247.